HHS Public Access

Author manuscript

Circulation. Author manuscript; available in PMC 2022 May 11.

Published in final edited form as:

Circulation. 2021 May 11; 143(19): 1894–1911. doi:10.1161/CIRCULATIONAHA.120.048698.

Increased ROS-mediated CaMKII activation contributes to calcium handling abnormalities and impaired contraction in Barth syndrome

Xujie Liu, PhD[1,2], **Suya Wang, PhD**[1], **Xiaoling Guo, PhD**[1,3], **Yifei Li, MD, PhD**[4], **Roza Ogurlu, BS**[1], **Fujian Lu, PhD**[1], **Maksymilian Prondzynski, PhD**[1], **Sofia de la Serna Buzon, PhD**[1], **Qing Ma, MD**[1], **Donghui Zhang, PhD**[5], **Gang Wang, MD, PhD**[1], **Justin Cotton, BS**[1,6], **Yuxuan Guo, PhD**[1], **Ling Xiao, PhD**[7], **David J. Milan, MD, PhD**[7], **Yang Xu, PhD**[8], **Michael Schlame, MD**[8], **Vassilios J. Bezzerides, MD, PhD**[1], **William T. Pu, MD**[1,9,*]

[1]Department of Cardiology, Boston Children's Hospital, Boston, MA 02115, USA

[2]Department of Radiology, Basic Medical School, Chongqing Medical University, Chongqing, 400016, China

[3]Center of Scientific Research, the Second Affiliated Hospital and Yuying Children's Hospital of Wenzhou Medical University, Wenzhou 325027, Zhejiang, China

[4]Key Laboratory of Birth Defects and Related Diseases of Women and Children of MOE, Department of Pediatrics, West China Second University Hospital, Sichuan University, Chengdu, Sichuan 610041, China

[5]State key laboratory of Biocatalysis and Enzyme Engineering, School of Life Science, Hubei University, Wuhan, Hubei 430062, China

[6]Harvard College, Cambridge, MA 02138, USA

[7]Department of Cardiology, Massachusetts General Hospital, Boston, MA 02114, USA

[8]Department of Anesthesiology, New York University School of Medicine, New York, New York.

[9]Harvard Stem Cell Institute, Cambridge, MA 02138, USA.

Abstract

Background: Mutations in tafazzin (*TAZ*), a gene required for biogenesis of cardiolipin, the signature phospholipid of the inner mitochondrial membrane, causes Barth syndrome (BTHS). Cardiomyopathy and risk of sudden cardiac death are prominent features of BTHS, but the mechanisms by which impaired cardiolipin biogenesis causes cardiac muscle weakness and arrhythmia are poorly understood.

[*]Correspondence to: William T. Pu, Department of Cardiology, Boston Children's Hospital, 300 Longwood Ave, Boston, MA 02115. william.pu@cardio.chboston.org.

CONFLICT OF INTEREST DISCLOSURES

WTP and VJB hold intellectual property on AAV-mediated inhibition of CaMKII for treatment of cardiac arrhythmias and for treatment of Barth syndrome, and are conducting research sponsored by Cydan and Sarepta on CaMKII inhibition for the treatment of catecholaminergic polymorphic ventricular tachycardia.

Methods: We performed in vivo electrophysiology to define arrhythmia vulnerability in cardiac specific *TAZ* knockout mice. Using cardiomyocytes derived from human induced pluripotent stem cells (iPSC-CMs) and cardiac specific *TAZ* knockout mice as model systems, we investigated the effect of *TAZ* inactivation on Ca^{2+} handling. Through genome editing and pharmacology, we defined a molecular link between *TAZ* mutation and abnormal Ca^{2+} handling and contractility.

Results: A subset of mice with cardiac-specific *TAZ* inactivation developed arrhythmias including bidirectional ventricular tachycardia, atrial tachycardia, and complete atrioventricular block. Compared to WT, BTHS iPSC-CMs had increased diastolic Ca^{2+} and decreased Ca^{2+} transient amplitude. BTHS iPSC-CMs had higher levels of mitochondrial and cellular ROS than WT, which activated Ca^{2+}/calmodulin-dependent protein kinase II (CaMKII). Activated CaMKII phosphorylated the cardiac ryanodine receptor (RYR2) on serine 2814, increasing Ca^{2+} leak through RYR2. Inhibition of this ROS-CaMKII-RYR2 pathway through pharmacological inhibitors or genome editing normalized aberrant Ca^{2+} handling in BTHS iPSC-CMs and improved their contractile function. Murine *Taz* knockout cardiomyocytes also exhibited elevated diastolic Ca^{2+} and decreased Ca^{2+} transient amplitude. These abnormalities were ameliorated by CaMKII or ROS inhibition.

Conclusions: This study identified a molecular pathway that links *TAZ* mutation to abnormal Ca^{2+} handling and decreased cardiomyocyte contractility. This pathway may offer therapeutic opportunities to treat BTHS and potentially other diseases with elevated mitochondrial ROS production.

Keywords

Barth syndrome; Ca^{2+} handling; iPSC-CMs; ROS; CaMKII; RYR2

INTRODUCTION

Cardiolipin, the signature phospholipid of the inner mitochondrial membrane, is required for the normal function of enzymes housed within this structure, most notably the electron transport chain and F1F0 ATP synthase.[1,2] Altered cardiolipin abundance and composition in heart failure have been hypothesized to impair mitochondrial function and contribute to cardiac dysfunction.[3,4] Study of Barth syndrome, the only known inherited disorder of cardiolipin metabolism, has provided critical insights into the biological function of cardiolipin. Barth syndrome is caused by mutation of the X-linked gene Tafazzin (*TAZ*)[5], which encodes a mitochondrial phospholipid-lysophospholipid transacylase responsible for the terminal step in the biogenesis of cardiolipin[6]. The major clinical features of Barth syndrome are cardiac and skeletal myopathy and neutropenia. Cardiomyopathy and sudden cardiac death are among the major clinical features that impact patient quality of life and survival[7–9].

The molecular mechanisms that connect *TAZ* deficiency to cardiomyopathy and sudden death are not clearly defined. Previously we integrated human induced pluripotent stem cell (iPSC)-derived cardiomyocytes (iPSC-CMs), genome editing, and ‘heart-on-a-chip’ technologies to model the cardiomyopathy of BTHS in a dish. We demonstrated that BTHS iPSC-CMs had high levels of reactive oxygen species (ROS)[10], which was confirmed in

TAZ-deficient murine cardiomyocytes[11]. BTHS iPSC-CM-based muscular thin films had impaired force generation, which was normalized by suppression of elevated ROS using the mitochondrially targeted ROS scavenger MitoTEMPO[10].

Intracellular Ca^{2+} is a critical regulator of cardiac rhythm and contraction. During the cardiomyocyte action potential, the L-type Ca^{2+} channel in the plasma membrane opens and allows entry of extracellular Ca^{2+}. This increase in cytoplasmic Ca^{2+} opens ryanodine receptor 2 (RYR2), located on the sarcoplasmic reticulum (SR), resulting in Ca^{2+}-induced Ca^{2+} release. The subsequent rapid increase in intracellular Ca^{2+} triggers sarcomere contraction. Inactivation of the L-type Ca^{2+} channel, closure of RYR2, and return of Ca^{2+} to the SR, via the activity of SERCA2a (sarcoplasmic/endoplasmic reticulum Ca^{2+}-ATPase 2a), and the extracellular space, via NCX1 (Na^{+}/Ca^{2+} exchanger), restores Ca^{2+} to its normal low levels in diastole, leading to sarcomere relaxation and preparing the cell for the next excitation-contraction cycle. Abnormal Ca^{2+} handling can impair cardiac contraction and relaxation and potentially precipitate lethal arrhythmias[12].

Here we tested the hypothesis that impaired Ca^{2+} handling contributes to cardiac dysfunction and arrhythmia in Barth syndrome by studying BTHS iPSC-CMs. We found that BTHS iPSC-CMs have reduced Ca^{2+} transient amplitude and elevated diastolic Ca^{2+}. We linked these abnormalities to excessive mitochondrial ROS production through activation of Ca^{2+}/calmodulin-dependent protein kinase II (CaMKII) and phosphorylation of RYR2 serine 2814 (RYR2-S2814). Finally, we demonstrate that inhibition of this ROS-CaMKII-RYR2 pathway ameliorated the abnormal Ca^{2+} handling and weak contraction of BTHS iPSC-CMs. Studies on murine TAZ knockout cardiomyocytes confirmed that these mechanisms are operative in bona fide cardiomyocytes. These results provide new insights into the links between mitochondrial dysfunction, ROS, abnormal Ca^{2+} handling, cardiac muscle weakness, and arrhythmia, and identify novel therapeutic avenues for BTHS.

MATERIALS AND METHODS

The authors declare that all supporting data are available within the article and its online supplementary files. Detailed Methods are available in the Supplemental Materials.

iPSC Culture, Differentiation and Treatment

PGP1 is a wild-type human male iPSC line that harbors a doxycycline (Dox)-inducible CRISPR/Cas9 transgene[10,13]. BTHH was derived from PGP1 using Dox-induced Cas9 genome editing[13] to introduce a *TAZ* frameshift mutation (c.517delG) found in a BTHS patient[10,13]. This patient's cells were also reprogrammed to yield an iPSC line, pBTHH[10]. The Dox-induced Cas9 genome editing strategy was used to introduce the same *TAZ* frameshift mutation into PGP1 harboring RYR2-S2814A (serine 2814 to alanine) mutations in both alleles[14] (herein named WT-S2814A), yielding BTHH-S2814A. Sequences and primers used in this study are provided in Table I in the Supplement. Normal karyotype was validated by either G-banded karyotyping or Nanostring karyotype assay (Fig. I–A in the Supplement).

Cardiomyocyte differentiation was induced as previously described[15,16] with minor modifications (Fig. I–B in the Supplement). iPSC-CM purity was measured by flow cytometry and immunofluorescent staining using primary antibodies shown in Table II in the Supplement.

Ca^{2+} Imaging

For ratiometric Ca^{2+} imaging, iPSC-CMs loaded with Fura-2 AM (Life Technologies) were recorded under 1 Hz pacing using the IonOptix Myocyte Calcium and Contractility System. The change in Fura-2 signal after addition of 10 mM caffeine was used to measure sarcoplasmic reticulum (SR) Ca^{2+} content. SR Ca^{2+} leak was measured as the tetracaine-induced reduction of Fluo-3 AM signal, as described previously[17]. For non-ratiometric Ca^{2+} imaging, cells were programmed to express GCaMP6f-Junctin (GCaMP6f-J) Ca^{2+} nanosensor, expressed from an adenovirus[18], or GCaMP5 lenti-virus (Addgene #46027)[19] and recorded by confocal line scan imaging (Olympus FV3000) or a Vala Biosciences Kinetic Image Cytometer (KIC).

Protein expression

Proteins were analyzed using the WES capillary western system (ProteinSimple). Primary antibodies are shown in Table II in the Supplement. HRP-conjugated secondary antibodies were from ProteinSimple. Total RYR2 was measured by enzyme-linked immunosorbent assay (ELISA; LifeSpan BioSciences, Inc.).

Contractility measurement

Engineered heart tissues (EHTs) were generated from iPSC-CMs (1E6 cells/EHT) as described[20] using iPSC-CMs treated with adenovirus that expressed ChR2-YFP[14]. EHTs were optically paced at 1 Hz at 37°C and recorded at 30 frames per second using a Keyence BZ-X Fluorescence Microscope with a 2x objective. Videos were analyzed using MuscleMotion[21].

Murine TAZ mice and knockout cardiomyocytes

Animal experiments were performed following protocols approved by Boston Children's Hospital Animal Care and Use Care Committee. Electrophysiology studies were performed as described previously[22]. *Taz*$^{flox/flox}$ mice on a C57BL/6J background were described previously[23]. Neonatal cardiomyocytes were isolated and purified using kits from Miltenyi Biotec. Cells were treated with adenovirus expressing either LacZ (Ad:LacZ; control) or Cre (Ad:Cre; Taz KO)[24]. *Taz*$^{flox/Y}$*; Myh6-Cre* (cardiomyocyte-specific *Taz* KO, CKO) and *Taz*$^{WT/Y}$*; Myh6-Cre* (control) mice were used for adult cardiomyocyte isolation by retrograde collagenase perfusion[25].

Statistical Analysis

Results are displayed as mean ± SD. Normally distributed data were analyzed with Welch's two-tailed *t*-test (two groups) or ANOVA with Dunnett's post hoc test (three or more groups). Otherwise, we used the Kruskal-Wallis test with Dunn's post hoc test or a permutation test. Values of $P < 0.05$ were considered significant.

RESULTS

In vivo arrhythmias in TAZ cardiac knockout mice

BTHS patients are at risk for sudden death[7–9]. Arrhythmia mechanisms are not well described, although case reports suggest vulnerability to ventricular tachycardia[26]. To better characterize arrhythmia vulnerability in *TAZ* deficiency, we performed electrophysiology studies on mice with cardiac specific *Taz* inactivation (CKO) at 6 weeks of age (Fig. 1A), when they had mild or no cardiac dysfunction (ref. [27] and Fig. II–A in the Supplement). Six of nine CKO mice had arrhythmias (Fig. 1B–D): two developed progressive atrioventricular node dysfunction that culminated in lethal complete heart block (Fig. II–B in the Supplement); two developed bidirectional ventricular tachycardia (VT) after adrenergic stimulation; one developed induced VT; and one developed induced atrial tachycardia. Among littermate controls, two of eight developed induced VT, which had much shorter duration than VT in CKO mice (Fig. 1E). The overall frequency of arrhythmias was greater in CKO, and, despite the small sample size and transient induced VT in two controls, this difference trended towards statistical significance (permutation test, P=0.096). These results suggest that cardiac *Taz* deficiency increases vulnerability to different types of arrhythmias. We were particularly interested in the vulnerability to bidirectional VT, given that this is an uncommon arrhythmia most closely linked to digitalis toxicity and catecholaminergic ventricular tachycardia[28], conditions that both involve elevated cytosolic Ca^{2+}.

iPSC-CM differentiation and metabolic characterization

iPSCs were efficiently differentiated to yield >70% $TNNT2^{+}$ iPSC-CMs (Figure I B–D in the Supplement), which exhibited robust contraction and Ca^{2+} transients (Video I in the Supplement). Most iPSC-CMs expressed ventricular cardiomyocyte marker MLC2V (HGNC: MYL2) and not immature/atrial cardiomyocyte marker MLC2A (HGNC: MYL7; Fig. I–E in the Supplement). The wild-type male human iPSC line PGP-1 was used as control (WT), and the PGP1-$TAZ^{c.517delG}$ line[10], generated from PGP-1 by genome editing (Fig. III–A in the Supplement), was used as the *TAZ* mutant line (BTHH). Sanger sequencing confirmed the single base pair frameshift mutation in the *TAZ* gene of BTHH (Fig. III–B in the Supplement), and capillary western demonstrated absence of TAZ protein in BTHH iPSC-CMs (Fig. III–C in the Supplement). Lipid mass spectrometry confirmed abnormal cardiolipin composition in BTHH iPSC-CMs (Fig. III–D in the Supplement). Mitochondrial networks, visualized by mitotracker green, demonstrated reduced branching number and branch length in BTHH iPSC-CMs compared to WT (Fig. III–E,F in the Supplement). Mitochondrial function, measured using an extracellular flux analyzer, was impaired in BTHH iPSC-CMs (Fig. III–G,H in the Supplement).

BTHH iPSC-CMs exhibit abnormal Ca^{2+} handling

To assess Ca^{2+} handling in BTHH iPSC-CMs, we loaded iPSC-CMs with the Ca^{2+} indicator Fura-2 and performed ratiometric Ca^{2+} imaging under electrical pacing at 1 Hz. Compared to WT, BTHH iPSC-CMs Ca^{2+} transient amplitude was lower by 30% and the diastolic Ca^{2+} concentration was higher by 34% (Fig. 2A–C). The maximal upstroke and recovery velocities of BTHH Ca^{2+} transients were significantly depressed compared to control (Fig.

2D and E). Similar abnormal Ca^{2+} handling was also observed in pBTHH iPSC-CMs, derived from a BTHS patient (Fig. IV–A in the Supplement).

Diastolic Ca^{2+} leak through RYR2, the major cardiomyocyte intracellular Ca^{2+} release channel, is a key determinant of cytoplasmic diastolic Ca^{2+} concentration. We quantified diastolic Ca^{2+} leak through RYR2 using the previously described “tetracaine shift” assay[17]. This showed that the diastolic Ca^{2+} leak through RYR2 was significantly greater in BTHH iPSC-CMs compared to WT (Fig. IV–B in the Supplement).

Increased Ca^{2+} leak through RYR2 often produces spontaneous Ca^{2+} release events known as Ca^{2+} sparks. To corroborate our finding of increased RYR2 Ca^{2+} leak, we measured Ca^{2+} sparks by using adenovirus to express a genetically encoded Ca^{2+} nanosensor, in which GCaMP6f is fused to Junctin, a protein that co-localizes with RYR2 in cardiomyocytes[18]. BTHH iPSC-CMs exhibited more frequent Ca^{2+} sparks (Fig. 2F, G). To better define the prevalence of aberrant Ca^{2+} release events, we used a higher throughput Ca^{2+} imaging system to record Ca^{2+} transients in a larger number of cells. The results confirmed that a much larger fraction of BTHH iPSC-CMs exhibited abnormal Ca^{2+} release events during pacing or immediately following pacing (Fig. IV–C–F in the Supplement).

Increased diastolic sarcoplasmic reticulum (SR) Ca^{2+} leak and reduced Ca^{2+} transient amplitude suggested the possibility of depleted SR Ca^{2+} stores. To test this hypothesis, after a standard pacing protocol, iPSC-CMs were treated with caffeine, which opens RYR2 and rapidly empties SR Ca^{2+} stores. BTHH iPSC-CMs showed significantly reduced caffeine-induced Ca^{2+} release compared to isogenic control iPSC-CMs (Fig. 2H and I), suggesting reduced SR Ca^{2+} stores.

ROS links TAZ mutation to abnormal Ca^{2+} handling in BTHH iPSC-CMs

We sought to delineate mechanisms by which deficiency of TAZ, a mitochondrial protein, induced elevated SR Ca^{2+} leak through RYR2. We previously showed that BTHS iPSC-CMs have elevated levels of mitochondrial ROS[10] and we hypothesized that high ROS levels in BTHS iPSC-CMs may contribute to abnormal Ca^{2+} handling.

We first confirmed that BTHH iPSC-CMs have elevated ROS by using flow cytometry to measure the mean fluorescence intensity of BTHH and WT mitochondria isolated from iPSC-CMs and stained with MitoSOX, a mitochondrially targeted, fluorescent ROS indicator (Fig. 3A). Elevated ROS was also detected at the level of whole cells in BTHH iPSC-CMs stained with CellROX, a whole cell fluorescent ROS probe (Fig. 3B). Consistent with these measurements, BTHH iPSC-CMs had elevated levels of 4-hydroxynonenal, a product of lipid peroxidation (Fig. 3C).

We next tested whether elevated ROS contributes to impaired Ca^{2+} handling in BTHH iPSC-CMs. To reduce ROS, we treated cells with the mitochondrially targeted ROS scavenger MitoTEMPO (MT). MT reduced ROS in BTHH iPSC-CMs (Fig. 3D). We then analyzed the effect of MT on iPSC-CM Ca^{2+} handling. MT treatment significantly improved Ca^{2+} transient amplitude and normalized diastolic Ca^{2+} concentration in BTHH iPSC-CMs (Fig. 3E and F). However, the Ca^{2+} transient maximal upstroke and recovery velocities were not

significantly changed (Fig. 3G and H). MT also reduced the high Ca^{2+} spark frequency observed in BTHH iPSC-CMs (Fig. IV–G in the Supplement). For comparison, we treated cells with *TAZ* modified mRNA (*TAZ* modRNA), which we previously showed rescues *TAZ* mutant iPSC-CM metabolic, structural, and contractile phenotypes[10]. *TAZ* modRNA corrected Ca^{2+} amplitude, diastolic Ca^{2+} concentration, and Ca^{2+} transient maximum upstroke velocity so that they were not significantly different between BTHH and WT (Fig. 3E–G), although it did not significantly correct the Ca^{2+} transient maximum recovery velocity (Fig. 3H). These data demonstrate that ROS is an essential intermediate that links TAZ deficiency to abnormal Ca^{2+} handling in BTHH iPSC-CMs. Less complete rescue by MT compared to *TAZ* modRNA suggests that either MT incompletely suppressed excessive ROS levels, or that both ROS-dependent and non-ROS dependent mechanisms contribute to the phenotype of *TAZ* mutant cells.

Excessive ROS induced CaMKII activation leads to abnormal Ca^{2+} handling in BTHH iPSC-CMs

CaMKII is a key kinase that modulates the activity of multiple Ca^{2+} handling proteins, including RYR2[29,30]. Following activation by calcified calmodulin, CaMKII oxidation or autophosphorylation locks CaMKII in an active form[30,31]. We hypothesized that elevated ROS activates CaMKII in BTHH iPSC-CMs and contributes to their Ca^{2+} handling abnormalities. To test this hypothesis, we measured CaMKII activation in BTHH and control iPSC-CMs using antibodies that detect phosphorylated, activated CaMKII (phosphorylated threonine 286; p-CaMKII), oxidized CaMKII (M281-M282 oxidation; ox-CaMKII), or total CaMKII. Capillary westerns showed that the ratio of p-CaMKII to total CaMKII (Fig. 4A) was significantly higher in BTHH iPSC-CMs. Furthermore, ox-CaMKII specific antibody demonstrated greater CaMKII oxidation in BTHH iPSC-CMs (Fig. 4B and Fig. V–A in the Supplement). To further assess CaMKII activity, we measured phospholamban (PLN) phosphorylation at Thr-17 (p-PLN), a well-established CaMKII phosphorylation site[32]. We observed that p-PLN (PLN monomer) was markedly elevated in BTHH iPSC-CMs (Fig. V–B in the Supplement), consistent with elevated CaMKII activity. Next, we assessed the effect of scavenging ROS by MT treatment on CaMKII activation in BTHH iPSC-CMs. Capillary westerns showed that MT treatment reduced ox-CaMKII levels in BTHH iPSC-CMs (Fig. V–C,D in the Supplement). The mean level of p-CaMKII was also lower in MT-treated BTHH iPSC-CMs, but this did not reach statistical significance due to substantial intra-group variation (Fig. V–C,D in the Supplement). Collectively, these data demonstrate that BTHH iPSC-CMs have elevated levels of activated forms of CaMKII (ox-CaMKII and p-CaMKII) and increased CaMKII activity, as reflected by greater p-PLN, and that CaMKII activation depends on increased mitochondrial ROS.

To evaluate the contribution of increased CaMKII activation to the Ca^{2+} handling abnormalities of BTHH iPSC-CMs, we treated iPSC-CMs with a cell permeable (myristoylated) form of autocamtide-2-related inhibitory peptide (AIP), a highly potent and selective CaMKII inhibitory peptide[33], and measured the effect on Ca^{2+} handling. AIP significantly but incompletely corrected BTHH iPSC-CM Ca^{2+} transient amplitude and reduced diastolic Ca^{2+} concentration to a level that was comparable to control (Fig. 4C–D). Maximal Ca^{2+} transient upstroke velocity of AIP-treated cells had an intermediate value,

such that it did not significantly differ from either control or BTHH iPSC-CMs (Fig. 4E). Max Ca^{2+} transient recovery velocity was not significantly affected by AIP (Fig. 4F). AIP treatment of BTHH iPSC-CMs also reduced the aberrant spontaneous Ca^{2+} release observed during or immediately after pacing (Fig. IV–E,F in the Supplement). Incomplete correction of Ca^{2+} transient amplitude and upstroke and recovery velocities may have been due to incomplete inhibition of CaMKII, or to a combination of both CaMKII-dependent and CaMKII-independent mechanisms that are responsible for the Ca^{2+} handling defects in *TAZ* mutant iPSC-CMs. Indeed, a prior study found that murine TAZ-deficient cardiomyocytes had reduced maximal SERCA2a activity linked to increased tyrosine nitration[34]. Consistent with this study, SERCA2a tyrosine nitration in BTHH iPSC-CMs tended to be higher than in WT ($p=0.09$; Fig. V–E–G in the Supplement). Other studies have demonstrated that elevated ROS can oxidize RYR2 and thereby increase aberrant Ca^{2+} release. To investigate whether this occurs in BTHH iPSC-CMs, we measured RYR2 oxidation using the monobromobimane (mBBr) assay (Fig. V–H,I in the Supplement). We did not detect a measurable difference in RYR2 oxidation between control and BTHH iPSC-CMs.

These data implicate mitochondrial ROS activation of CaMKII in the aberrant Ca^{2+} handling of TAZ-deficient iPSC-CMs. Other mechanisms, such as SERCA2a nitration, likely also contribute to the Ca^{2+} handling phenotype.

RYR2 phosphorylation by CaMKII contributes to abnormal Ca^{2+} handling in TAZ mutant iPSC-CMs

Among the Ca^{2+} handling proteins phosphorylated by CaMKII is RYR2. CaMKII-mediated RYR2 phosphorylation at serine 2814 (RYR2-pS2814) increases RYR2 diastolic Ca^{2+} leak, promotes arrhythmia, and adversely impacts myocardial outcome in heart disease models[35,36]. Our data indicate elevated diastolic Ca^{2+} concentration in conjunction with elevated RYR2 Ca^{2+} flux (Fig. 3F and Fig. IV–A,B in the Supplement) and ROS-dependent CaMKII activation in BTHH iPSC-CMs. These findings led us to evaluate the contribution of CaMKII-mediated RYR2 at serine 2814[29] to abnormal Ca^{2+} handling in BTHH iPSC-CMs. RYR2-pS2814 immunoreactivity was markedly elevated in BTHH iPSC-CMs, whereas total RYR2 expression levels detected by ELISA were unchanged (Fig. 5A).

To delineate the contribution of elevated RYR2-pS2814 to Ca^{2+} handling abnormalities of BTHH iPSC-CMs, we used Cas9 genome editing to ablate this phosphosite by converting serine 2814 to alanine in both *RYR2* alleles in the context of wild-type or mutant *TAZ*. We confirmed successful genome editing in the WT-S2814A and BTHH-S2814A iPSC lines by Sanger sequencing of the target loci (Fig. 5B). We did not detect off-target genome modification (Table III in the Supplement). Immunoblotting confirmed loss of RYR2-S2814 phosphorylation (Fig. 5C).

We used ratiometric Ca^{2+} imaging to measure Ca^{2+} transients in BTHH-S2814A and WT-S2814A. In cells with functional TAZ, S2814A mutation did not significantly affect Ca^{2+} handling (Fig. 5D–G; Fig. IV–G in the Supplement). In contrast, in cells with mutant *TAZ*, ablation of the RYR2-S2814 phosphorylation site increased and maximal Ca^{2+} transient upstroke velocity and reduced diastolic Ca^{2+} concentration (Fig. 5D–F). RYR2-S2814A mutation also reduced Ca^{2+} spark frequency of *TAZ* mutant iPSC-CMs (Fig.

IV–G in the Supplement). Indeed, diastolic Ca^{2+} concentration and maximal Ca^{2+} transient upstroke velocity became indistinguishable from control cells, suggesting that CaMKII-mediated phosphorylation of RYR2-S2814 plays a predominant role in the derangement of these parameters in *TAZ* mutant cells. However, Ca^{2+} transient amplitude and Ca^{2+} spark frequency were incompletely corrected, and Ca^{2+} transient recovery velocity was not significantly changed (Fig. 5G), suggesting that additional CaMKII targets, or CaMKII-independent mechanisms, contribute to these abnormalities.

Collectively, these results indicate that ROS-mediated CaMKII activation, RYR2-S2814 phosphorylation, and elevated diastolic RYR2 Ca^{2+} flux contribute to abnormal Ca^{2+} handling in BTHH iPSC-CMs.

Activated ROS-CaMKII-RYR2 pathway induced Ca^{2+} abnormalities in Taz mutant murine cardiomyocytes

The immaturity of iPSC-CMs can raise questions as to the extent to which observed abnormalities translate to bona fide cardiomyocytes. Therefore, to complement the human iPSC-CMs studies, we studied cardiomyocytes isolated from Taz^{flox} mice, in which loxP elements flank exons 5 to 10.

We first studied ventricular cardiomyocytes prepared from $Taz^{flox/Y}$ (male) neonatal mice. We treated isolated neonatal murine ventricular cardiomyocytes (NMVMs) prepared from these mice with adenovirus that expressed either Cre (Ad:Cre; *Taz* ablated) or LacZ (Ad:LacZ; control). Capillary western confirmed efficient *Taz* ablation after treatment with Ad:Cre at a multiplicity of infection of 20 (Fig. VI–A in the Supplement). Ad:Cre treated NMVMs had higher levels of ROS than Ad:LacZ controls (Fig. 6A). As in BTHH iPSC-CMs, Ad:Cre-treated NMVMs showed significantly higher levels of ox-CaMKII (Fig. VI–B,C in the Supplement). However, the level of p-CaMKII did not differ significantly from control (Fig. VI-B,C in the Supplement). RYR2-pS2814 was markedly elevated and total RYR2 was not significantly altered in *Taz*-deficient NMVMs compared to controls (Fig. 6B). These data support ROS-mediated CaMKII activation and RYR2-pS2814 phosphorylation in *Taz* mutant NMVMs.

To evaluate Ca^{2+} handling in *Taz* mutant and control NMVMs, we performed ratiometric Ca^{2+} imaging (Fig. 6C–F, Fig. VI–D in the Supplement). Consistent with our observations in *TAZ* mutant iPSC-CMs, *Taz*-ablated NMVMs had significantly lower Ca^{2+} transient amplitude and reduced maximal Ca^{2+} transient upstroke velocity (Fig. 6C, E). Diastolic Ca^{2+} concentration also tended to be elevated in *Taz* mutant NMVMs ($p=0.051$; Fig. 6D). However, unlike the iPSC-CM model, maximal Ca^{2+} transient recovery velocity was not significantly changed in *Taz* mutant NMVMs (Fig. 6F). Thus *Taz* mutant NMVMs exhibited abnormal Ca^{2+} handling that was largely consistent with the abnormalities observed in BTHH iPSC-CMs.

We next evaluated the effect of reducing ROS levels with MT or inhibiting CaMKII with AIP on Ca^{2+} handling of control and *Taz* mutant NMVMs. Consistent with the results from iPSC-CMs, both MT and AIP corrected the Ca^{2+} transient amplitude, diastolic Ca^{2+} concentration, and maximal Ca^{2+} transient upstroke velocity of *Taz* mutant NMVMs so they

became indistinguishable from control values (Fig. 6C–F). These results mechanistically implicate mitochondrial ROS and CaMKII activation in the aberrant Ca^{2+} handling of *Taz* mutant NMVMs.

Ca^{2+} handling of cardiomyocytes changes substantially during the first weeks of postnatal life. Therefore we also studied the Ca^{2+} handling of *Taz* mutant (*Myh6Cre*$^{+}$*; Taz*$^{fl/Y}$) and control (*Myh6Cre*$^{-}$*;Taz*$^{fl/Y}$) adult murine ventricular cardiomyocytes (AMVMs). Using both CellRox staining and ELISA to measure levels of the lipid peroxidation product 4-HNE, we confirmed elevated levels of ROS in *Taz* mutant AMVMs (Fig. 7A and Fig. VI–E in the Supplement). By capillary western, ox-CaMKII tended to be elevated in *Taz* mutant AMVMs (p=0.077; Fig. VI–F,G in the Supplement). Mean p-CaMKII to total CaMKII ratio was elevated in *Taz* mutant AMVMs, although this observation did not reach statistical significance (Fig. VI–F,G in the Supplement). *Taz* mutant AMVMs also had significantly elevated phosphorylation of CaMKII targets RYR2-pS2814 (Fig. 7B) And PLN-pT17 (Fig. VI–H in the Supplement).

Ratiometric Ca^{2+} imaging demonstrated that the *Taz* mutant AMVMs had Ca^{2+} handling defects similar to those observed in iPSC-CMs (Fig. 7C–F, Fig. VI–D in the Supplement): reduced Ca^{2+} transient amplitude, elevated diastolic Ca^{2+} concentration, and lower maximal Ca^{2+} transient recovery velocity. However, Ca^{2+} transient maximal upstroke velocity was not significantly altered. Inhibition of CaMKII by AIP tended to increase the Ca^{2+} transient amplitude (p=0.058; Fig. 7C) and significantly reduced the diastolic Ca^{2+} concentration (Fig. 7D). However, AIP treatment of *Taz* mutant AMVMs did not significantly correct the maximal Ca^{2+} transient recovery velocity and did not significantly affect the maximal Ca^{2+} upstroke velocity (Fig. 7E, F).

Together these data demonstrate that *Taz* mutant, bona fide murine cardiomyocytes have Ca^{2+} handling abnormalities that are largely consistent with those observed in iPSC-CMs and that are ameliorated by reduction of ROS or inhibition of CaMKII.

Normalization Ca^{2+} handling improves BTHH EHT contractile function

Ca^{2+} is the central mediator of excitation-contraction coupling. Reduced Ca^{2+} transient amplitude and Ca^{2+} upstroke velocity, and elevated diastolic Ca^{2+}, impair cardiomyocyte contraction and relaxation, respectively. To investigate a potential link between aberrant Ca^{2+} handling and contractile dysfunction in Barth syndrome, we assembled control or BTHH iPSC-CMs, transduced with the optogenetic actuator ChR2-YFP, into engineered heart tissues (EHTs; Fig. VII–A in the Supplement). BTHH iPSC-CMs cultured on a stiff, two-dimensional, patterned substrate exhibited defective sarcomere organization[10]. In the three dimensional EHT context, both control and BTHH iPSC-CMs displayed elongated, aligned morphology and well organized sarcomeres (Fig. VII–B,C in the Supplement), indicating that the EHT culture conditions enabled cells to overcome barriers to sarcomere assembly posed by TAZ deficiency in the cell patterning assay[10]. Nevertheless, BTHH EHTs showed weaker contraction than controls (3.7-fold reduction; Fig. 8A; Video II in the Supplement), consistent with our prior studies of *TAZ* mutant muscular thin films[10].

We studied the effect of *TAZ* replacement by *TAZ* modRNA, ROS scavenging by MT, and CaMKII inhibition by AIP on BTHH EHT contraction (Fig. 8B). *TAZ* modRNA, MT, or AIP treatments did not alter the contractile function of control EHTs (Fig. 8C–E). In contrast, *TAZ* modRNA markedly improved the contraction of BTHH EHTs by 3.7-fold (Fig. 8F; Video III in the Supplement), indicating that the contractile defects are largely reversible by gene replacement. Scavenging ROS with MT partially restored contractile function (2.4-fold, Fig. 8G; Video IV in the Supplement), although not to the same level as *TAZ* modRNA (Fig. 8F). Treatment of EHTs with AIP also improved contractile function (1.5-fold; Fig. 8H; Video V in the Supplement), although the effect was weaker than that of *TAZ* modRNA or MT.

We further evaluated the effect of *TAZ* mutation on AMVM contraction, using edge detection to measure sarcomere length during the contraction of dissociated cardiomyocytes. *TAZ* mutant (*Myh6Cre; Taz*$^{fl/Y}$) and control cardiomyocytes were isolated from 2-month-old mice, when the mutant mice have mild cardiac dysfunction[27]. Consistent with the EHT model, individual *TAZ* mutant cardiomyocytes had reduced contraction amplitude ($P<0.01$) and relaxation velocity ($P<0.05$; Fig. 8I–L). Treatment with AIP to inhibit CaMKII tended to increase contraction amplitude ($P=0.093$), shortening velocity ($P=0.055$), and relaxation velocity ($P=0.081$; Fig. 8J–L). These data suggest that TAZ deficiency contributes to impaired contraction of individual cardiomyocytes and implicate excessive CaMKII activation as a factor in *TAZ* mutant cardiomyocyte dysfunction.

DISCUSSION

BTHS patients have cardiomyopathy and risk of sudden cardiac death from incompletely described arrhythmias[7–9,26]. Here we studied mice with cardiac-restricted *Taz* knockout and show that a subset developed complete heart block, atrial tachycardia, and bidirectional VT, which were not observed in wild-type controls. The significance of complete heart block after anesthesia and catheter placement but before drug treatment or ventricular stimulation is uncertain, as some vulnerable mice develop this arrhythmia non-specifically under anesthesia, and progressive functional heart block has not been reported to our knowledge in Barth syndrome patients. On the other hand, VT requiring ICD placement occurs in some Barth patients[7–9,26]. A subset of Barth mice developed bidirectional VT under adrenergic stimulation. This arrhythmia is closely associated with dysregulated Ca^{2+} handling in digitalis toxicity and catecholaminergic polymorphic VT due to mutations in *RYR2*[28]. In the latter condition, we recently demonstrated that RYR2-S2814 phosphorylation by CaMKII is a critical event that unmasks latent arrhythmia mutations during catecholamine stimulation[14,22]. Our results suggest that in Barth syndrome, ROS-mediated CaMKII activation drives excessive RYR2-S2814 phosphorylation, predisposing hearts to development of bidirectional VT. Unfortunately the low penetrance of VT in this model will make it difficult to use for therapeutic trials of anti-arrhtyhmic efficacy.

The mechanisms that lead from *TAZ* mutation to contractile dysfunction and arrhythmia are incompletely understood. Diminished energy reserves may contribute to baseline cardiac dysfunction and limited augmentation of heart function with exercise in BTHS patients[37]. iPSC-CMs successfully model aspects of the BTHS cardiomyopathy phenotype[10,38]. In

iPSC-CMs, the cardiomyopathy phenotype was corrected by normalization of ROS levels with MitoTEMPO, but not by culture conditions that normalized ATP levels.[10] Here we demonstrate that elevated ROS in BTHS iPSC-CMs and murine cardiomyocytes activates CaMKII and impairs Ca^{2+} handling, which could contribute to both cardiac dysfunction and arrhythmias.

Oxidative stress is well established to exacerbate cardiac dysfunction and predispose to arrhythmias. A key mediator of these deleterious effects of ROS is CaMKII, which can be "locked" in an activated state by oxidation of methionine 281/282[30,31]. Here, we link mitochondrial ROS production in *TAZ* mutant cardiomyocytes to CaMKII activation. *TAZ* mutation likely elevates mitochondrial ROS through at least two mechanisms. First, *TAZ* mutation destabilizes electron transport chain supercomplexes by impairing the biogenesis of cardiolipin, which is required for supercomplex assembly[38–41]. Second, *TAZ* mutation impairs mitophagy, thereby reducing mitochondrial quality control[42]. Extension of excessive ROS into the cytoplasm, likely in the form of hydrogen peroxide, activates CaMKII and exposes the myocardium to its associated deleterious outcomes. The mechanism likely extends to other forms of mitochondrial disease which trigger increased levels of oxidative stress.

Our identification of a ROS-CaMKII pathway that is active in the pathogenesis of cardiac disease in BTHS suggests that antagonizing this pathway may be a productive therapeutic strategy. In mice with partial *TAZ* depletion induced by shRNA against *TAZ*, elevated ROS levels were detected, but expression of mitochondrially targeted catalase did not affect cardiac function[11]. However, these mice did not exhibit cardiac dysfunction and cardiac rhythm was not investigated, so it was not possible to evaluate the contribution of ROS to pathogenesis of this phenotype. CaMKII activation has been implicated in the pathogenesis of multiple forms of heart disease and arrhythmia.[43,44] Our studies suggest that CaMKII inhibition may improve heart function and ameliorate arrhythmia in BTHS and potentially other mitochondrial myopathies with elevated ROS production. However, it is important to note that CaMKII inhibition only partially rescued most phenotypes, possibly from a combination of incomplete inhibition and important contributions of CaMKII-independent mechanisms, including increased tyrosine nitrosylation of SERCA2a. Among potential additional mechanisms are other kinases activated downstream of oxidative stress, including Mitogen Activated Protein Kinases, Protein Kinase A, some Protein Kinase C isoforms, Protein Kinase D, and Protein Kinase G, and direct oxidation or nitrosylation of key biomolecules, including sarcomeric proteins such as titin[45].

Across the iPSC-CM and murine *TAZ* mutant models that we studied, a common feature was elevated diastolic Ca^{2+} concentration. Elevated diastolic Ca^{2+} concentration was associated with increased diastolic Ca^{2+} leak through RYR2 and was fully corrected by suppression of ROS, inhibition of CaMKII, and ablation of the RYR2-S2814 CaMKII phosphosite, which is known to increase RYR2 diastolic Ca^{2+} leak[36]. These data strongly implicate ROS–CaMKII–RYR2-S2814 phosphorylation as a primary mechanism underlying elevation of diastolic Ca^{2+} in *TAZ* mutant cardiomyocytes. Elevated diastolic Ca^{2+} impairs cardiac relaxation[46] and promotes cardiac arrhythmias[12], phenotypes observed in some BTHS patients. Additional studies are needed to fully test this hypothesis and to evaluate

whether interruption of this signaling pathway can ameliorate these disease phenotypes in BTHS animal models and patients.

In conclusion, our studies identify Ca^{2+} handling abnormalities in both human iPSC-derived and murine cardiomyocytes with *TAZ* mutation. We show that ROS-mediated activation of CaMKII contributes to the pathogenesis of aberrant Ca^{2+} handling in BTHS. These mechanistic insights suggest therapeutic approaches to cardiac dysfunction and arrhythmia in BTHS and possibly other mitochondrial cardiomyopathies. Since cardiolipin abnormalities are also observed in acquired heart disease[3,4], the mechanisms revealed by this study may also contribute to the pathogenesis of more prevalent forms of heart disease.

Supplementary Material

Refer to Web version on PubMed Central for supplementary material.

ACKNOWLEDGEMENTS

XL designed the study, performed experiments, and analyzed data. SW, YL, and QM contributed to the mouse experiments. SdlSB and VJB performed and analyzed mouse electrophysiology experiments. GW provided reagents and conceptual insights. XG, DZ, and JC contributed to iPSC-CM culture and characterization. MP contributed to EHT studies. YX and MS performed cardiolipin mass spectrometry. RO, FL, DJM, LX, and VJB contributed to cardiomyocyte physiology experiments and analysis. XL wrote the manuscript. WTP provided oversight for the project and edited the manuscript.

FUNDING SOURCES

WTP was supported by NIH grants HL128694 and UG3TR002145 and the Barth Syndrome Foundation. MS was supported by NIH grant R01GM115593.

NONSTANDARD ABBREVIATIONS AND ACRONYMS:

AIP	Autocamtide-2-related inhibitory peptide
AMVMs	Adult murine ventricular cardiomyocytes
BTHS	Barth syndrome
CaMKII	Ca^{2+}/calmodulin-dependent protein kinase II
Ctrl	Control
EHT	Engineered heart tissue
iPSC	Induced pluripotent stem cells
iPSC-CMs	iPSC-derived cardiomyocytes
KO	Knockout
mBBr	Monobromobimane
MT	MitoTEMPO
RFP	Red fluorescent protein

ROS	Reactive oxygen species
RYR2	Ryanodine receptor 2
SR	Sarcoplasmic reticulum
Veh	Vehicle

REFERENCES

1. Ren M, Phoon CKL, Schlame M. Metabolism and function of mitochondrial cardiolipin. Prog Lipid Res. 2014;55C:1–16.
2. Raja V, Greenberg ML. The functions of cardiolipin in cellular metabolism-potential modifiers of the Barth syndrome phenotype. Chem Phys Lipids. 2014;179:49–56. [PubMed: 24445246]
3. Sabbah HN. Targeting the Mitochondria in Heart Failure: A Translational Perspective. JACC: Basic to Translational Science. 2020;5:88–106. [PubMed: 32043022]
4. Chicco AJ, Sparagna GC. Role of cardiolipin alterations in mitochondrial dysfunction and disease. Am J Physiol Cell Physiol. 2007;292:C33–44. [PubMed: 16899548]
5. Bione S, D'Adamo P, Maestrini E, Gedeon AK, Bolhuis PA, Toniolo D. A novel X-linked gene, G4.5. is responsible for Barth syndrome. Nat Genet. 1996;12:385–389. [PubMed: 8630491]
6. Saric A, Andreau K, Armand A-S, Møller IM, Petit PX. Barth Syndrome: From Mitochondrial Dysfunctions Associated with Aberrant Production of Reactive Oxygen Species to Pluripotent Stem Cell Studies. Front Genet. 2015;6:359. [PubMed: 26834781]
7. Clarke SLN, Bowron A, Gonzalez IL, Groves SJ, Newbury-Ecob R, Clayton N, Martin RP, Tsai-Goodman B, Garratt V, Ashworth M, et al. Barth syndrome. Orphanet J Rare Dis. 2013;8:23. [PubMed: 23398819]
8. Roberts AE, Nixon C, Steward CG, Gauvreau K, Maisenbacher M, Fletcher M, Geva J, Byrne BJ, Spencer CT. The Barth Syndrome Registry: distinguishing disease characteristics and growth data from a longitudinal study. Am J Med Genet A. 2012;158A:2726–2732. [PubMed: 23045169]
9. Spencer CT, Bryant RM, Day J, Gonzalez IL, Colan SD, Thompson WR, Berthy J, Redfearn SP, Byrne BJ. Cardiac and clinical phenotype in Barth syndrome. Pediatrics. 2006;118:e337–46. [PubMed: 16847078]
10. Wang G, McCain ML, Yang L, He A, Pasqualini FS, Agarwal A, Yuan H, Jiang D, Zhang D, Zangi L, et al. Modeling the mitochondrial cardiomyopathy of Barth syndrome with induced pluripotent stem cell and heart-on-chip technologies. Nat Med. 2014;20:616–623. [PubMed: 24813252]
11. Johnson JM, Ferrara PJ, Verkerke ARP, Coleman CB, Wentzler EJ, Neufer PD, Kew KA, de Castro Brás LE, Funai K. Targeted overexpression of catalase to mitochondria does not prevent cardioskeletal myopathy in Barth syndrome. J Mol Cell Cardiol. 2018;121:94–102. [PubMed: 30008435]
12. Landstrom AP, Dobrev D, Wehrens XHT. Calcium Signaling and Cardiac Arrhythmias. Circ Res. 2017;120:1969–1993. [PubMed: 28596175]
13. Wang G, Yang L, Grishin D, Rios X, Ye LY, Hu Y, Li K, Zhang D, Church GM, Pu WT. Efficient, footprint-free human iPSC genome editing by consolidation of Cas9/CRISPR and piggyBac technologies. Nat Protoc. 2017;12:88–103. [PubMed: 27929521]
14. Park S-J, Zhang D, Qi Y, Li Y, Lee KY, Bezzerides VJ, Yang P, Xia S, Kim SL, Liu X, et al. Insights Into the Pathogenesis of Catecholaminergic Polymorphic Ventricular Tachycardia From Engineered Human Heart Tissue. Circulation. 2019;140:390–404. [PubMed: 31311300]
15. Lian X, Hsiao C, Wilson G, Zhu K, Hazeltine LB, Azarin SM, Raval KK, Zhang J, Kamp TJ, Palecek SP. Robust cardiomyocyte differentiation from human pluripotent stem cells via temporal modulation of canonical Wnt signaling. Proc Natl Acad Sci U S A. 2012;109:E1848–57. [PubMed: 22645348]
16. Lian X, Zhang J, Azarin SM, Zhu K, Hazeltine LB, Bao X, Hsiao C, Kamp TJ, Palecek SP. Directed cardiomyocyte differentiation from human pluripotent stem cells by modulating

Wnt/β-catenin signaling under fully defined conditions. Nat Protoc. 2013;8:162–175. [PubMed: 23257984]

17. Shannon TR, Ginsburg KS, Bers DM. Quantitative assessment of the SR Ca2+ leak-load relationship. Circ Res. 2002;91:594–600. [PubMed: 12364387]
18. Shang W, Lu F, Sun T, Xu J, Li L-L, Wang Y, Wang G, Chen L, Wang X, Cannell MB, et al. Imaging Ca2+ nanosparks in heart with a new targeted biosensor. Circ Res. 2014;114:412–420. [PubMed: 24257462]
19. Addis RC, Ifkovits JL, Pinto F, Kellam LD, Esteso P, Rentschler S, Christoforou N, Epstein JA, Gearhart JD. Optimization of direct fibroblast reprogramming to cardiomyocytes using calcium activity as a functional measure of success. J Mol Cell Cardiol. 2013;60:97–106. [PubMed: 23591016]
20. Breckwoldt K, Letuffe-Brenière D, Mannhardt I, Schulze T, Ulmer B, Werner T, Benzin A, Klampe B, Reinsch MC, Laufer S, et al. Differentiation of cardiomyocytes and generation of human engineered heart tissue. Nat Protoc. 2017;12:1177–1197. [PubMed: 28492526]
21. Sala L, van Meer BJ, Tertoolen LGJ, Bakkers J, Bellin M, Davis RP, Denning C, Dieben MAE, Eschenhagen T, Giacomelli E, et al. MUSCLEMOTION: A Versatile Open Software Tool to Quantify Cardiomyocyte and Cardiac Muscle Contraction In Vitro and In Vivo. Circ Res. 2018;122:e5–e16. [PubMed: 29282212]
22. Bezzerides VJ, Caballero A, Wang S, Ai Y, Hylind RJ, Lu F, Heims-Waldron DA, Chambers KD, Zhang D, Abrams DJ, et al. Gene Therapy for Catecholaminergic Polymorphic Ventricular Tachycardia by Inhibition of Ca2+/Calmodulin-Dependent Kinase II. Circulation. 2019;140:405–419. [PubMed: 31155924]
23. Ren M, Xu Y, Erdjument-Bromage H, Donelian A, Phoon CKL, Terada N, Strathdee D, Neubert TA, Schlame M. Extramitochondrial cardiolipin suggests a novel function of mitochondria in spermatogenesis. J Cell Biol. 2019;218:1491–1502. [PubMed: 30914420]
24. Lin Z, Zhou P, von Gise A, Gu F, Ma Q, Chen J, Guo H, van Gorp PRR, Wang D-Z, Pu WT. Pi3kcb links Hippo-YAP and PI3K-AKT signaling pathways to promote cardiomyocyte proliferation and survival. Circ Res. 2015;116:35–45. [PubMed: 25249570]
25. Li D, Wu J, Bai Y, Zhao X, Liu L. Isolation and culture of adult mouse cardiomyocytes for cell signaling and in vitro cardiac hypertrophy. J Vis Exp [Internet]. 2014;Available from: 10.3791/51357
26. Spencer CT, Byrne BJ, Gewitz MH, Wechsler SB, Kao AC, Gerstenfeld EP, Merliss AD, Carboni MP, Bryant RM. Ventricular arrhythmia in the X-linked cardiomyopathy Barth syndrome. Pediatr Cardiol. 2005;26:632–637. [PubMed: 16235007]
27. Wang S, Li Y, Xu Y, Ma Q, Lin Z, Schlame M, Bezzerides VJ, Strathdee D, Pu WT. AAV Gene Therapy Prevents and Reverses Heart Failure in a Murine Knockout Model of Barth Syndrome. Circ Res. 2020;126:1024–1039. [PubMed: 32146862]
28. Leenhardt A, Denjoy I, Guicheney P. Catecholaminergic polymorphic ventricular tachycardia. Circ Arrhythm Electrophysiol. 2012;5:1044–1052. [PubMed: 23022705]
29. Wehrens XHT, Lehnart SE, Reiken SR, Marks AR. Ca2+/calmodulin-dependent protein kinase II phosphorylation regulates the cardiac ryanodine receptor. Circ Res. 2004;94:e61–e70. [PubMed: 15016728]
30. Erickson JR, He BJ, Grumbach IM, Anderson ME. CaMKII in the cardiovascular system: sensing redox states. Physiol Rev. 2011;91:889–915. [PubMed: 21742790]
31. Erickson JR, Joiner M-LAL, Guan X, Kutschke W, Yang J, Oddis CV, Bartlett RK, Lowe JS, O'Donnell SE, Aykin-Burns N, et al. A dynamic pathway for calcium-independent activation of CaMKII by methionine oxidation. Cell. 2008;133:462–474. [PubMed: 18455987]
32. Mattiazzi A, Mundiña-Weilenmann C, Guoxiang C, Vittone L, Kranias E. Role of phospholamban phosphorylation on Thr17 in cardiac physiological and pathological conditions. Cardiovasc Res. 2005;68:366–375. [PubMed: 16226237]
33. Ishida A, Kameshita I, Okuno S, Kitani T, Fujisawa H. A novel highly specific and potent inhibitor of calmodulin-dependent protein kinase II. Biochem Biophys Res Commun. 1995;212:806–812. [PubMed: 7626114]

34. Braun JL, Hamstra SI, Messner HN, Fajardo VA. SERCA2a tyrosine nitration coincides with impairments in maximal SERCA activity in left ventricles from tafazzin-deficient mice. Physiol Rep. 2019;7:e14215. [PubMed: 31444868]
35. Respress JL, van Oort RJ, Li N, Rolim N, Dixit SS, deAlmeida A, Voigt N, Lawrence WS, Skapura DG, Skårdal K, et al. Role of RyR2 phosphorylation at S2814 during heart failure progression. Circ Res. 2012;110:1474–1483. [PubMed: 22511749]
36. van Oort RJ, McCauley MD, Dixit SS, Pereira L, Yang Y, Respress JL, Wang Q, De Almeida AC, Skapura DG, Anderson ME, et al. Ryanodine receptor phosphorylation by calcium/calmodulin-dependent protein kinase II promotes life-threatening ventricular arrhythmias in mice with heart failure. Circulation. 2010;122:2669–2679. [PubMed: 21098440]
37. Bashir A, Bohnert KL, Reeds DN, Peterson LR, Bittel AJ, de Las Fuentes L, Pacak CA, Byrne BJ, Cade WT. Impaired cardiac and skeletal muscle bioenergetics in children, adolescents, and young adults with Barth syndrome. Physiol Rep [Internet]. 2017;5. Available from: 10.14814/phy2.13130
38. Dudek J, Cheng I-F, Balleininger M, Vaz FM, Streckfuss-Bömeke K, Hübscher D, Vukotic M, Wanders RJA, Rehling P, Guan K. Cardiolipin deficiency affects respiratory chain function and organization in an induced pluripotent stem cell model of Barth syndrome. Stem Cell Res. 2013;11:806–819. [PubMed: 23792436]
39. Gonzalvez F, D'Aurelio M, Boutant M, Moustapha A, Puech J-P, Landes T, Arnauné-Pelloquin L, Vial G, Taleux N, Slomianny C, et al. Barth syndrome: Cellular compensation of mitochondrial dysfunction and apoptosis inhibition due to changes in cardiolipin remodeling linked to tafazzin (TAZ) gene mutation [Internet]. Biochimica et Biophysica Acta (BBA) - Molecular Basis of Disease. 2013;1832:1194–1206. Available from: 10.1016/j.bbadis.2013.03.005 [PubMed: 23523468]
40. Zhang M, Mileykovskaya E, Dowhan W. Gluing the respiratory chain together. Cardiolipin is required for supercomplex formation in the inner mitochondrial membrane. J Biol Chem. 2002;277:43553–43556. [PubMed: 12364341]
41. Pfeiffer K, Gohil V, Stuart RA, Hunte C, Brandt U, Greenberg ML, Schägger H. Cardiolipin stabilizes respiratory chain supercomplexes. J Biol Chem. 2003;278:52873–52880. [PubMed: 14561769]
42. Hsu P, Liu X, Zhang J, Wang H-G, Ye J-M, Shi Y. Cardiolipin remodeling by TAZ/tafazzin is selectively required for the initiation of mitophagy. Autophagy. 2015;11:643–652. [PubMed: 25919711]
43. Anderson ME, Brown JH, Bers DM. CaMKII in myocardial hypertrophy and heart failure. J Mol Cell Cardiol. 2011;51:468–473. [PubMed: 21276796]
44. Bezzerides VJ, Prondzynski M, Carrier L, Pu WT. Gene therapy for inherited arrhythmias. Cardiovasc Res. 2020;116:1635–1650. [PubMed: 32321160]
45. Steinberg SF. Oxidative stress and sarcomeric proteins. Circ Res. 2013;112:393–405. [PubMed: 23329794]
46. Eisner David A, Caldwell Jessica L, Trafford Andrew W, Hutchings David C The Control of Diastolic Calcium in the Heart. Circ Res. 2020;126:395–412. [PubMed: 31999537]
47. Tohyama S, Hattori F, Sano M, Hishiki T, Nagahata Y, Matsuura T, Hashimoto H, Suzuki T, Yamashita H, Satoh Y, et al. Distinct metabolic flow enables large-scale purification of mouse and human pluripotent stem cell-derived cardiomyocytes. Cell Stem Cell. 2013;12:127–137. [PubMed: 23168164]
48. Sharma A, Toepfer CN, Schmid M, Garfinkel AC, Seidman CE. Differentiation and Contractile Analysis of GFP-Sarcomere Reporter hiPSC-Cardiomyocytes. Curr Protoc Hum Genet. 2018;96:21.12.1–21.12.12.
49. Sun G, Yang K, Zhao Z, Guan S, Han X, Gross RW. Matrix-Assisted Laser Desorption/Ionization Time-of-Flight Mass Spectrometric Analysis of Cellular Glycerophospholipids Enabled by Multiplexed Solvent Dependent Analyte−Matrix Interactions [Internet]. Analytical Chemistry. 2008;80:7576–7585. Available from: 10.1021/ac801200w [PubMed: 18767869]
50. Xu Y, Phoon CKL, Berno B, D'Souza K, Hoedt E, Zhang G, Neubert TA, Epand RM, Ren M, Schlame M. Loss of protein association causes cardiolipin degradation in Barth syndrome. Nat Chem Biol. 2016;12:641–647. [PubMed: 27348092]

51. Oda T, Yang Y, Uchinoumi H, Thomas DD, Chen-Izu Y, Kato T, Yamamoto T, Yano M, Cornea RL, Bers DM. Oxidation of ryanodine receptor (RyR) and calmodulin enhance Ca release and pathologically alter, RyR structure and calmodulin affinity. J Mol Cell Cardiol. 2015;85:240–248. [PubMed: 26092277]

52. Yang J, Zhang R, Jiang X, Lv J, Li Y, Ye H, Liu W, Wang G, Zhang C, Zheng N, et al. Toll-like receptor 4–induced ryanodine receptor 2 oxidation and sarcoplasmic reticulum Ca2+ leakage promote cardiac contractile dysfunction in sepsis. J Biol Chem. 2018;293:794–807. [PubMed: 29150444]

53. Terentyev D, Györke I, Belevych AE, Terentyeva R, Sridhar A, Nishijima Y, de Blanco EC, Khanna S, Sen CK, Cardounel AJ, et al. Redox modification of ryanodine receptors contributes to sarcoplasmic reticulum Ca2+ leak in chronic heart failure. Circ Res. 2008;103:1466–1472. [PubMed: 19008475]

54. Guo A, Song L-S. AutoTT: automated detection and analysis of T-tubule architecture in cardiomyocytes. Biophys J. 2014;106:2729–2736. [PubMed: 24940790]

55. von Gise A, Lin Z, Schlegelmilch K, Honor LB, Pan GM, Buck JN, Ma Q, Ishiwata T, Zhou B, Camargo FD, et al. YAP1, the nuclear target of Hippo signaling, stimulates heart growth through cardiomyocyte proliferation but not hypertrophy. Proc Natl Acad Sci U S A. 2012;109:2394–2399. [PubMed: 22308401]

56. Agah R, Frenkel PA, French BA, Michael LH, Overbeek PA, Schneider MD. Gene recombination in postmitotic cells. Targeted expression of Cre recombinase provokes cardiac-restricted, site-specific rearrangement in adult ventricular muscle in vivo. J Clin Invest. 1997;100:169–179. [PubMed: 9202069]

CLINICAL PERSPECTIVE

What is new?

1. *TAZ* mutant hearts are vulnerable to complete heart block and ventricular tachycardia.
2. *TAZ* deficient cardiomyocytes have abnormal Ca^{2+} handling.
3. A ROS-CaMKII-RYR2 molecular pathway links *TAZ* mutation to abnormal Ca^{2+} handling in BTHS iPSC-CMs, which contributes to decreased cardiomyocyte contractile function.

What Are the Clinical Implications?

1. Evaluation of BTHS patients for ventricular tachycardia and dynamic heart block is warranted.
2. Abnormal Ca^{2+} handling observed in BTHS iPSC-CMs may contribute to cardiac dysfunction and arrhythmia in BTHS patients.
3. Manipulation of the identified ROS-CaMKII-RYR2 pathway therapeutic opportunities for BTHS and potentially other forms of heart disease with elevated mitochondrial ROS production.

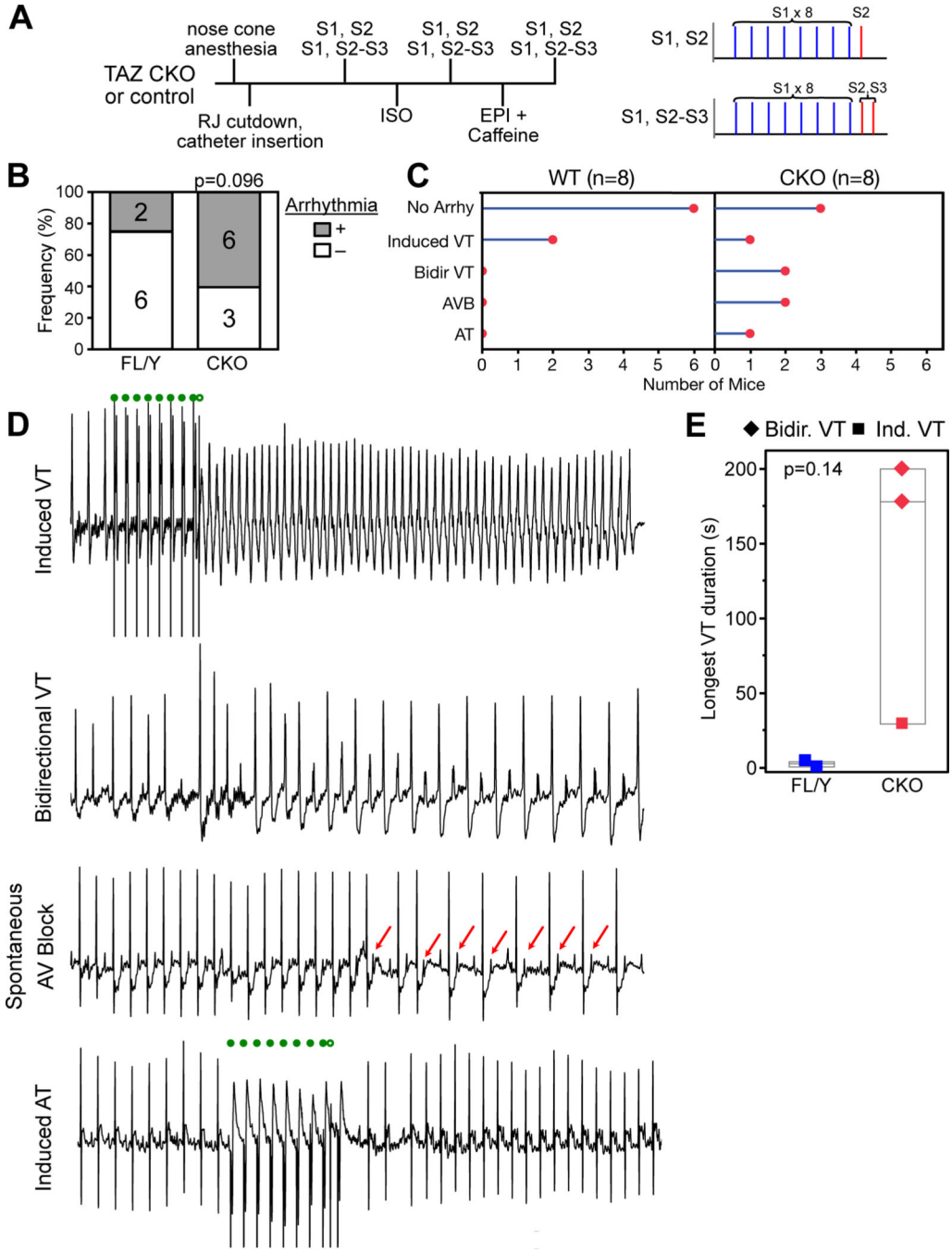

Figure 1. Cardiac arrhythmias in TAZ CKO mice.

Male control (*Taz*$^{FL/Y}$) or cardiac-specific mutant mice (CKO, *Myh6-Cre*; *Taz*$^{FL/Y}$) underwent intracardiac EP study at 6 weeks of age. Studies and analyses were performed blinded to genotype. **A.** Schematic of electrophysiology study protocol. **B.** Fraction of mice with arrhythmia. Numbers indicate sample sizes. Permutation test. **C.** Classification of types of arrhythmia within each genotype. **D.** Representative surface electrocardiograms demonstrating types of arrhythmias observed in CKO. Filled and open green circles indicate S1-S2 programmed ventricular stimulation. Red arrows highlight non-conducted p-waves.

Bidirectional VT was induced by treatment with epinephrine and caffeine. **E.** Longest duration of VT. VT duration was greater in CKO mice, although this was not statistically significant at these low sample sizes. Permutation test.

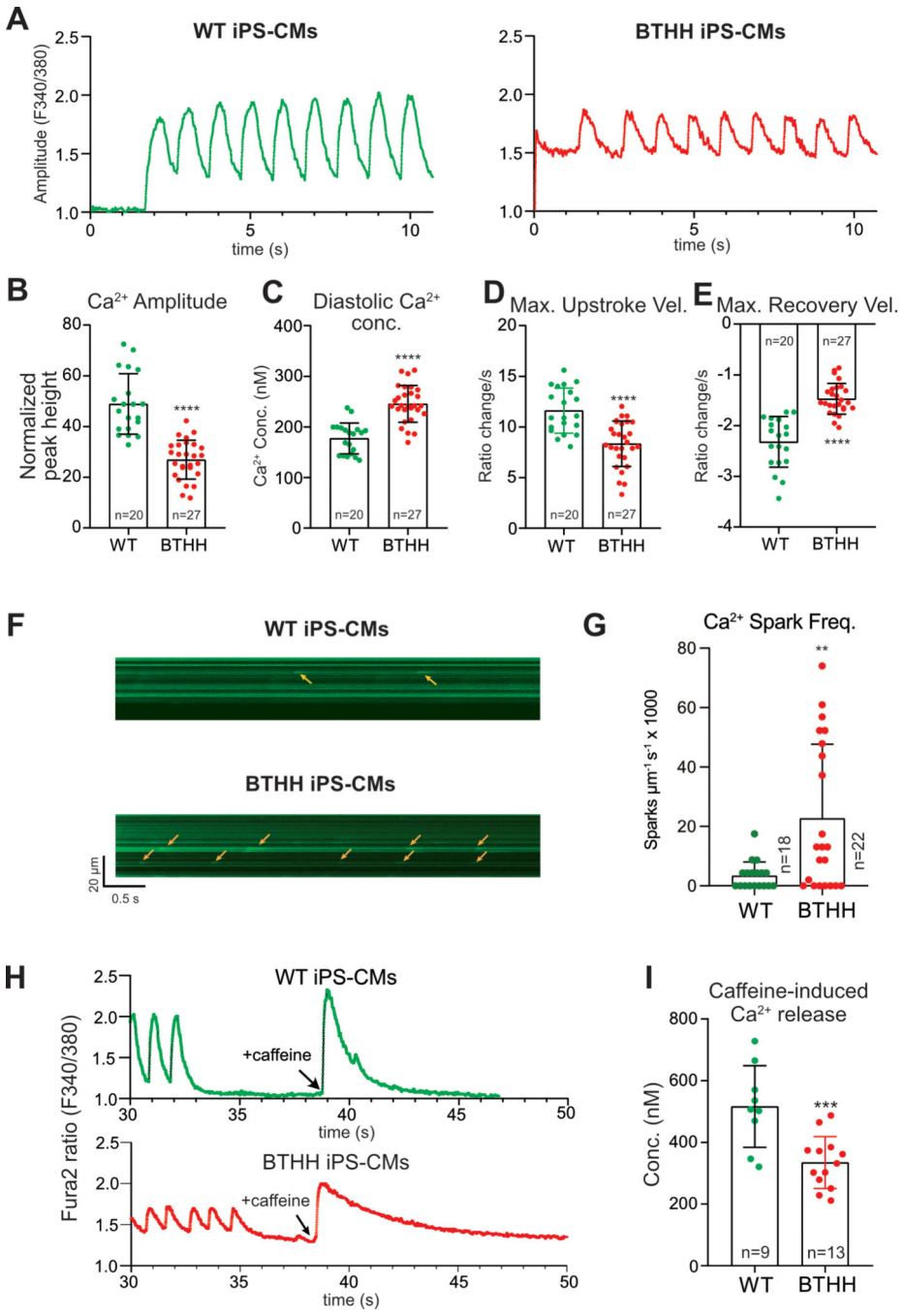

Figure 2. Abnormal Ca^{2+} handling in BTHH iPSC-CMs.

A. Representative Ca^{2+} transients of WT and BTHH iPSC-CMs imaged by Fura-2. Cells were electrically paced at 1 Hz. **B–E.** Quantitative analysis of the Ca^{2+} transient amplitude, diastolic Ca^{2+} concentration, and maximal Ca^{2+} upstroke and recovery velocities of WT and BTHH iPSC-CMs paced at 1 Hz. Each dot represents a different cell cluster. **F-G.** Ca^{2+} sparks in BTHH and WT iPSC-CMs cells. iPSC-CMs expressing a GCaMP6f-Junctin Ca^{2+} nano-sensor[18] were paced at 1 Hz. Ca^{2+} sparks were recorded by confocal line scan imaging (F). Yellow arrows, Ca^{2+} sparks. Quantitative analysis (G) showed that Ca^{2+} spark

frequency was significantly higher in BTHH compared to WT. n indicates number of cells studied. **H-I**. SR Ca^{2+} stores were measured by quantifying caffeine-induced Ca^{2+} release in Fura-2-loaded iPSC-CMs. H, representative Ca^{2+} transient traces of caffeine-induced Ca^{2+} transient. I, quantitative analysis of caffeine-induced Ca^{2+} release in BTHH compared to WT. Two-tailed *t*-test: ** $P<0.01$, *** $P<0.001$, **** $P<0.0001$.

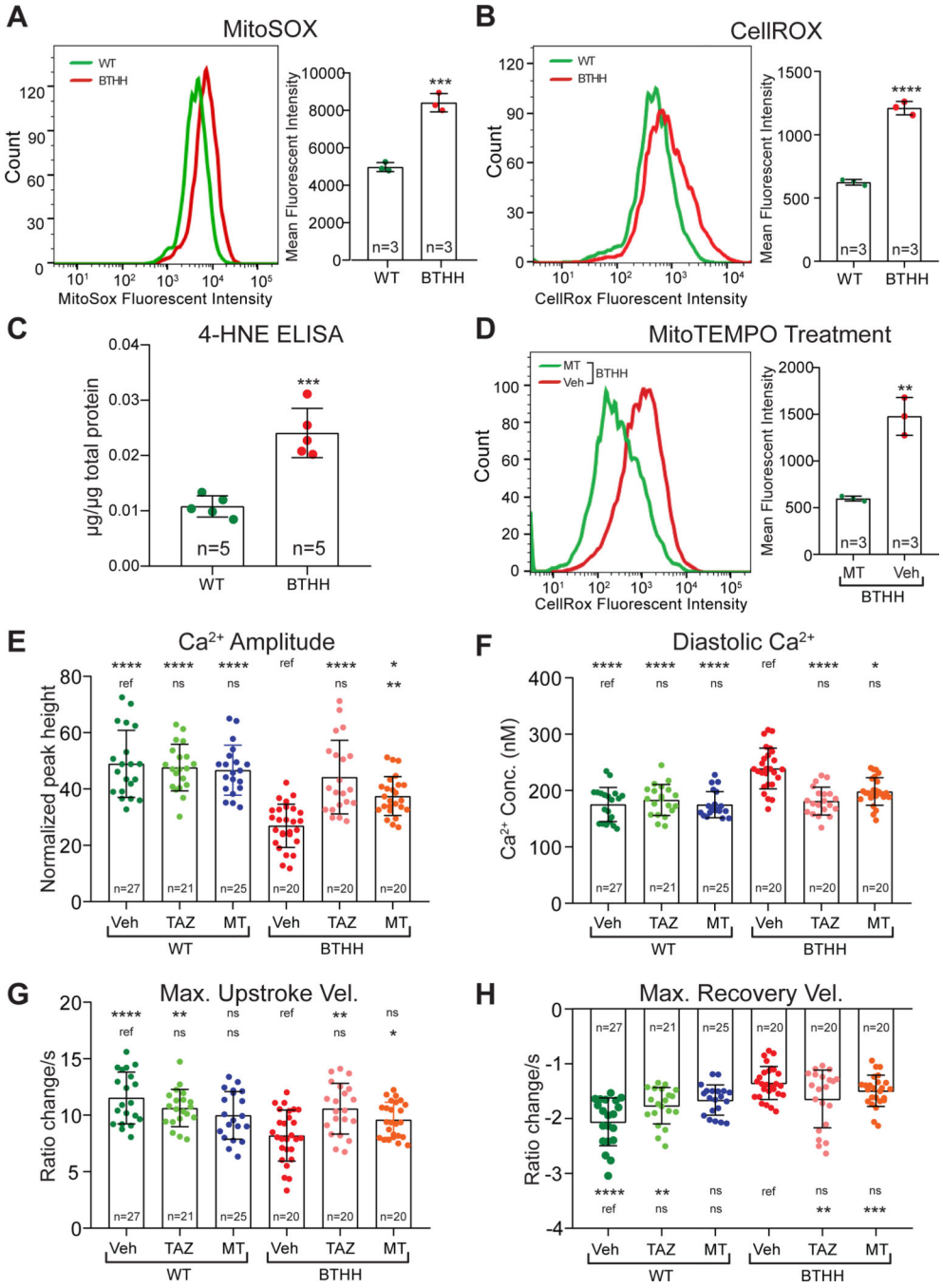

Figure 3. Elevated ROS in *TAZ* mutant iPSC-CMs contributes to abnormal Ca^{2+} handling.

A-B. Mitochondrial or cellular ROS levels in BTHH and WT iPSC-CMs were measured by flow cytometry of mitochondria stained with MitoSOX (A) or cells stained with CellROX (B), respectively. **C**. Levels of the lipid peroxidation product 4-HNE were detected in BTHH and WT iPSC-CMs by ELISA. **D**. MitoTEMPO (MT) treatment reduced ROS levels in BTHH iPSC-CMs to WT levels. **E-H.** Effect of MT or *TAZ* modRNA on BTHH iPSC-CM Ca^{2+} handling. Fura-2 loaded iPSC-CMs were electrically paced at 1 Hz and analyzed by ratiometric Ca^{2+} imaging. Comparisons were to either mock-treated BTHH or mock-treated

WT, as indicated by the labelled reference (ref.), using Kruskal-Wallis with Dunn's multiple comparison test. * $P<0.05$, ** $P<0.01$, *** $P<0.001$, **** $P<0.0001$. ns, not significant.

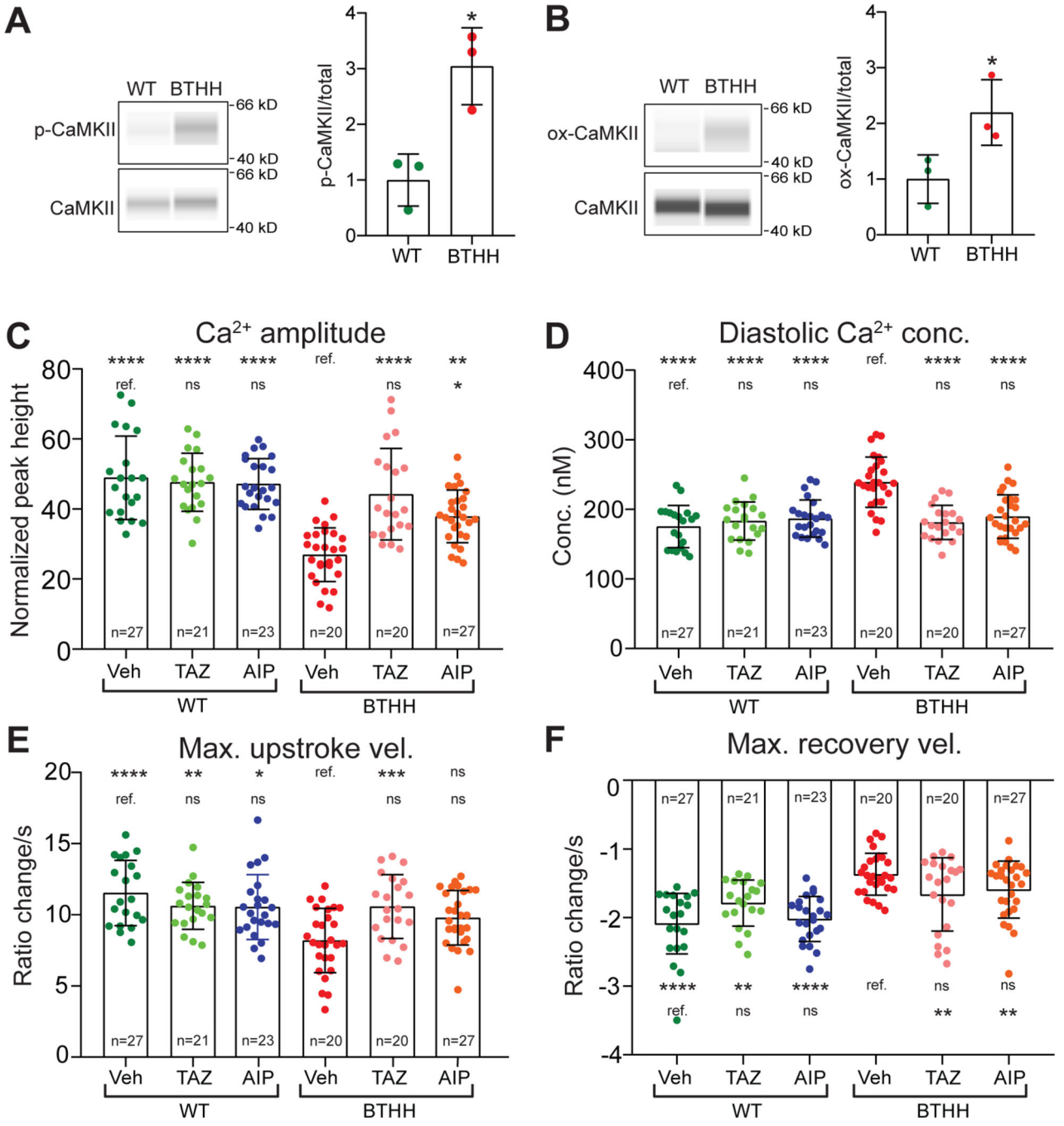

Figure 4. CaMKII activation promotes aberrant Ca^{2+} handling in *TAZ* mutant iPSC-CMs.

A,B. Capillary westerns for phosphorylated (Thr286), oxidized (M281/M282), and total CaMKII, in WT and BTHH iPSC-CMs. Left, representative virtual blot images; Right, quantification. *T*-test. **C-F.** Effect of CaMKII inhibition on BTHH iPSC-CM Ca^{2+} handling. Fura-2 loaded iPSC-CMs were electrically paced at 1 Hz and analyzed by ratiometric Ca^{2+} imaging. Data for vehicle and *TAZ* modRNA groups, statistical analysis, and symbols are the same as in Fig. 3E–H.

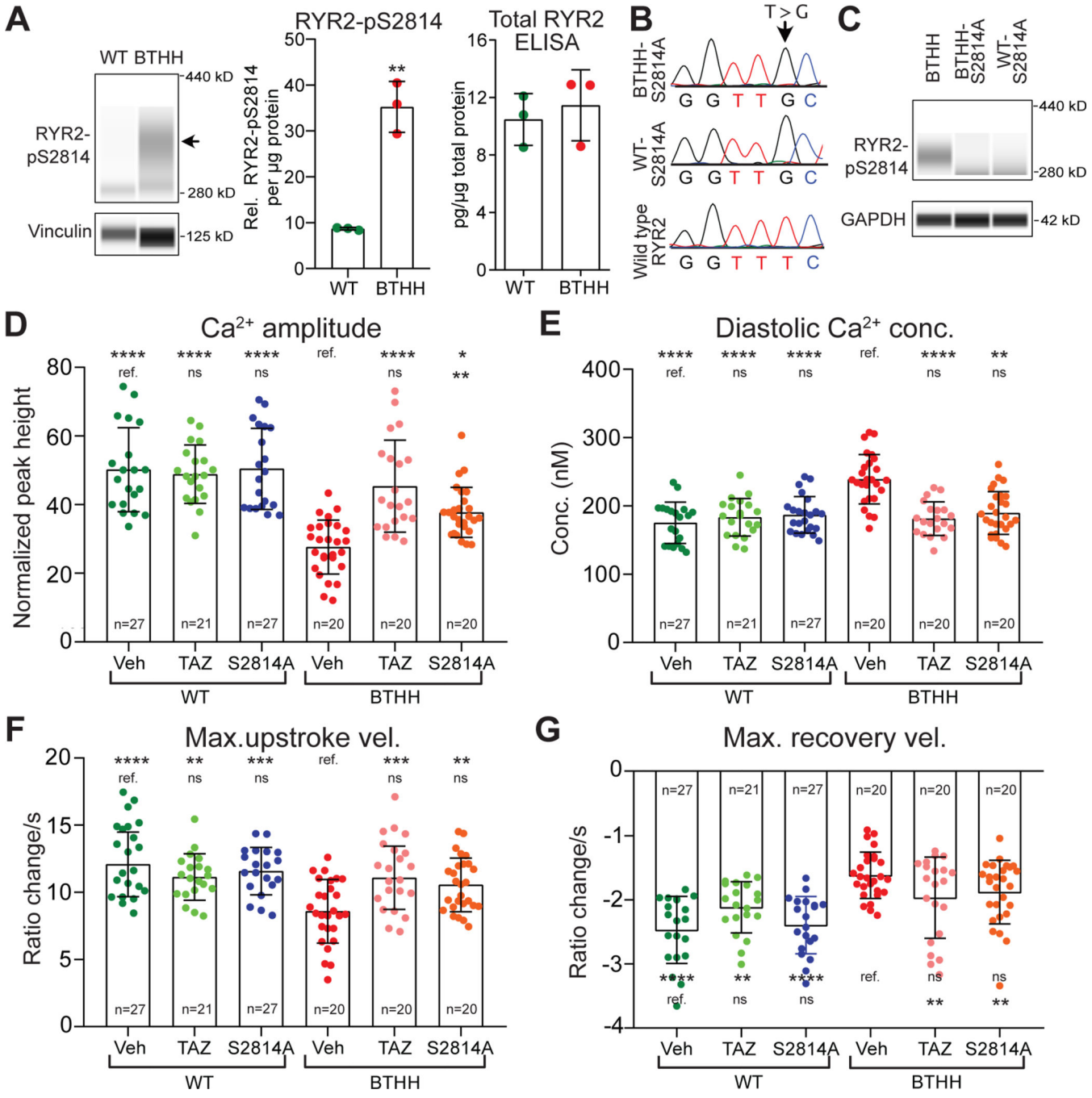

Figure 5. RYR2 phosphorylation contributes to abnormal Ca^{2+} handling in *TAZ* mutant iPSC-CMs.

A. Elevated RYR2-pS2814 in BTHH iPSC-CMs. The level of RYR2 phosphorylated at S2814 was measured by capillary western. Left, representative virtual image. Arrow, RYR2-pS2814 band. Middle, quantitative analysis of RYR2-pS2814 in BTHH and WT. Right, measurement of total RYR2 by ELISA. Two-tailed *t*-test. **B**. Homozygous mutation of RYR2 to convert S2814 to alanine. Dox-induced Cas9 genome editing was used to ablate the RYR2 S2814 phosphosites. Sanger sequencing of a genomic DNA amplicon confirmed

successful mutation of both RYR2 alleles in WT and BTHH iPSCs. **C**. Loss of RYR2-S2814 phosphorylation in WT/BTHH-S2814A iPSC-CMs was confirmed by immunoblotting. BTHH iPSC-CMs were used as a positive control. **D-G.** Effect of RYR2 S2814A mutation on BTHH and WT Ca^{2+} handling. Fura-2 loaded iPSC-CMs were electrically paced at 1 Hz and analyzed by ratiometric Ca^{2+} imaging. Data for vehicle and *TAZ* modRNA groups, statistical analysis, and symbols are the same as in Fig. 3E–H.

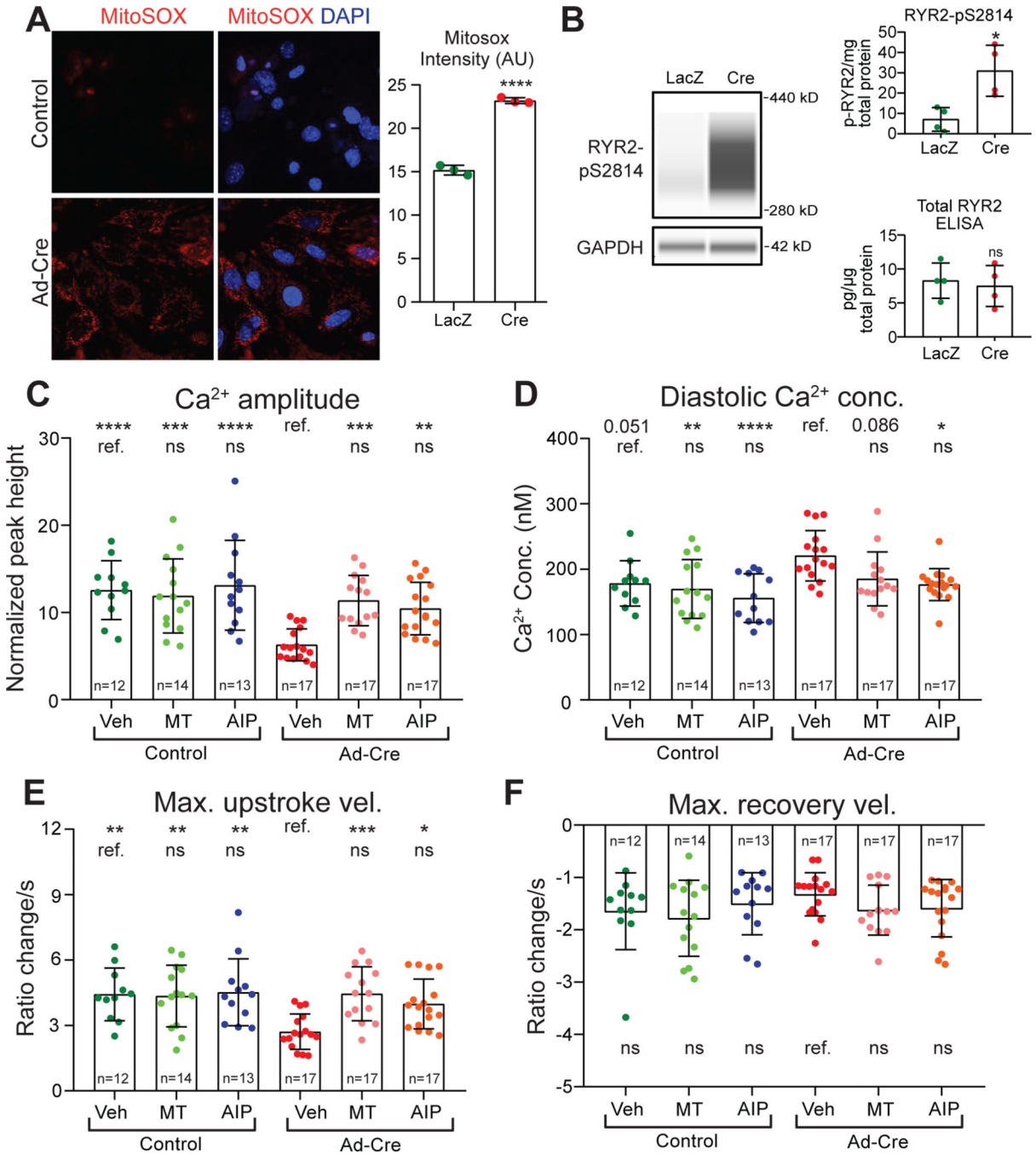

Figure 6. Abnormal Ca^{2+} handling in Taz KO neonatal mouse ventricular cardiomyocytes.

A. Mitochondrial ROS levels in control and *Taz*-ablated neonatal mouse ventricular cardiomyocytes. Cultured $Taz^{fl/fl}$ neonatal mouse ventricular cardiomyocytes were treated with Ad-Cre or Ad-LacZ. 3 days later they were stained with MitoSox and DAPI. Left, representative image. Right, quantitative analysis of the mean fluorescence intensity of three randomly acquired fields per group. Two-tailed *t*-test. B. RYR2-S2814 phosphorylation in *Taz* mutant or control NMVMs. Left, representative virtual capillary western image. Top right, quantification of capillary western measurement of RYR2-pS2814. Bottom right,

ELISA quantification of total RYR2 level. Two-tailed *t*-test. C-F. Effect of ROS scavenger (MT) or CaMKII inhibition (AIP) on Ca^{2+} transients in *Taz* KO and control NMVMs. Fura-2 loaded NMVMs were electrically paced at 1 Hz and analyzed by ratiometric Ca^{2+} imaging. Only Ca^{2+} transient amplitude fit a normal distribution and was analyzed by ANOVA with Dunnett's multiple comparison test, whereas the remaining parameters were analyzed by Kruskal-Wallis with Dunn's multiple comparison test. Comparisons were to either mock-treated *Taz* KO or mock-treated WT, as indicated by the labelled reference (ref.) group in each row. * $P<0.05$, ** $P<0.01$, *** $P<0.001$, **** $P<0.0001$. ns, not significant.

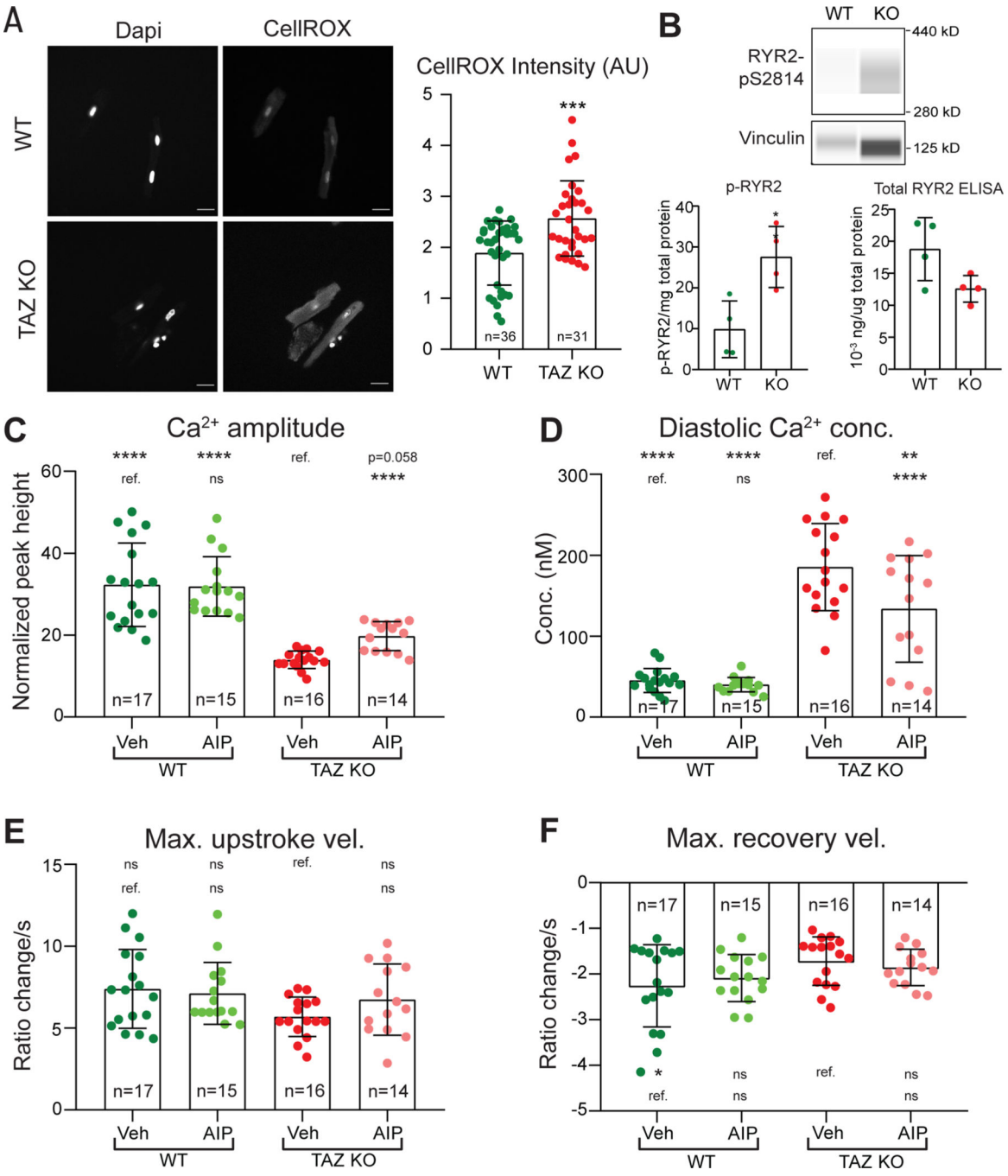

Figure 7. Abnormal Ca^{2+} handling in adult *Taz* KO mice ventricular cardiomyocytes.

A. ROS levels in isolated *Taz* KO and control AMVMs. Cells were stained with CellROX. Left, representative images. Right, quantification. Each point represents one cell. Two-tailed *t*-test. **B**. RYR2-S2814 phosphorylation in *Taz* KO and control AMVMs. RYR2-pS2814 was measured by capillary western. Top, capillary western virtual image. Bottom left, RYR2-pS2814 quantification. Bottom right, total RYR2 quantification by ELISA. Two-tailed *t*-test. **C-F.** Ca^{2+} transient parameters of *Taz* KO and control AMVMs. Two-month-old *Taz* KO ($Myh6Cre^{+}$; $TAZ^{fl/Y}$) and control AMVMs were dissociated, loaded with Fura-2, and

analyzed using ratiometric Ca^{2+} imaging with 1Hz pacing and AIP or vehicle treatment. Maximal Ca^{2+} upstroke velocities were analyzed with Kruskal-Wallis with Dunn's multiple comparison test, whereas the remaining parameters were analyzed by ANOVA with Dunnett's multiple comparison test. Comparisons were to either vehicle treated *Taz* KO or WT, as indicated by the labelled reference group (ref.) in each row. * $P<0.05$, ** $P<0.01$, *** $P<0.001$, **** $P<0.0001$. ns, not significant.

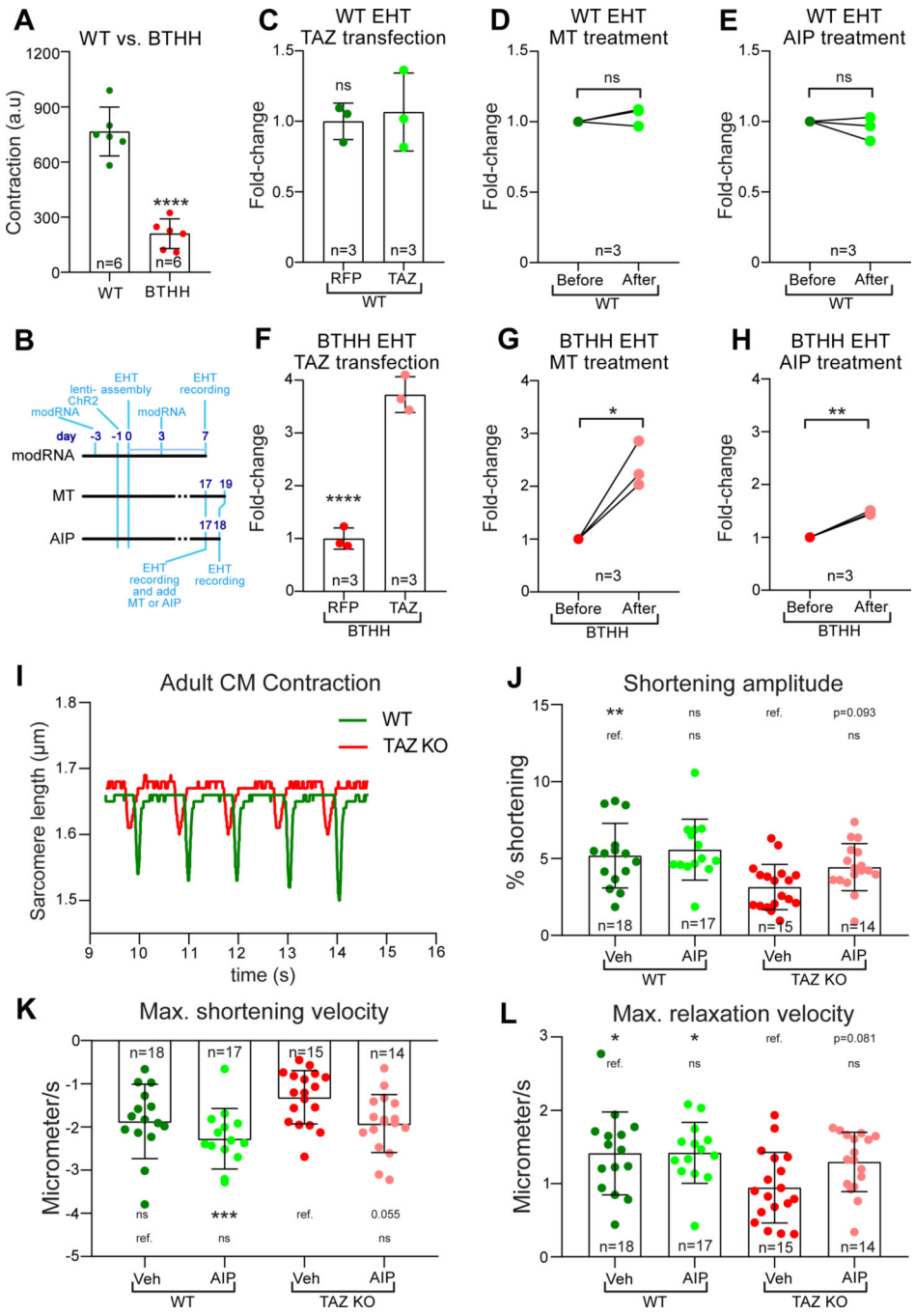

Figure 8. Inhibition of ROS-CaMKII-RYR2 pathway restored contractile function of *TAZ* mutant cardiomyocytes.

A. Reduced contractile function of BTHH EHTs compared to controls. BTHH or control iPSC-CMs were assembled into EHTs. Contractile function was measured at 14 days after EHTs started contracting using MuscleMotion. a.u., arbitrary units. Two-tailed *t*-test. **B-H.** Effect of *TAZ* modRNA, MT, or AIP on control or BTHH EHT contractile function. B, experimental timelines. *TAZ* or RFP modRNA iPSC-CMs were assembled into EHTs. EHTs were treated again with *TAZ* or RFP modRNA on day 3. EHTs were assayed on day 7. Two-

tailed *t*-test. For MT or AIP experiments, EHTs were assayed on day 17 prior to treatment. EHTs were then treated with AIP or MT for 1 or 2 days, respectively, and then assayed again. Relative contractile function is expressed as fold-change compared to pre-treatment values. Paired *t*-test. C, F. TAZ modRNA treatment of WT or BTHH EHTs. D,G. MT treatment of WT or BTHH EHTs. E,H. AIP treatment of WT or BTHH EHTs. **I-L.** Effect of *TAZ* mutation and CaMKII inhibition on AMVM contractile function. CMs were isolated from 2-month-old *Taz* KO (*Myh6Cre*$^{+}$; *Taz*$^{fl/Y}$) or control hearts. Contractile function of individual myocytes was measured by video measurement of sarcomere length. I, representative traces of WT and *Taz* KO sarcomere length during 1 Hz pacing. J, Fractional shortening of *Taz* KO and control cardiomyocytes treated for 2 hours with vehicle or AIP. K-L, maximal velocity of shortening or relaxation of WT and *Taz* KO cardiomyocytes. Maximal shortening velocity did not fit a normal distribution and was analyzed with Kruskal-Wallis with Dunn's multiple comparison test, whereas the remaining parameters were analyzed by ANOVA with Dunnett's multiple comparison test. Comparisons were to either mock-treated BTHH or mock-treated WT, as indicated by the labelled reference (ref.) group in each row. * $P<0.05$, ** $P<0.01$, *** $P<0.001$, **** $P<0.0001$. ns, not significant.